Novel Approach for Sizing Forward Osmosis Membrane Systems

Sourav Mondal[a], R Field[b], Jun Jie Wu[c]

[a] *Mathematical Institute, University of Oxford, Oxford OX2 6GG, UK*

[b] *Department of Engineering Science, University of Oxford, Oxford OX1 3PJ, UK*

[c] *School of Engineering and Computing Sciences, Durham University, Durham DH1 3LE, UK*

Abstract

Analytical solutions for sizing ideal Forward Osmosis membrane systems are developed for both co-current and counter-current flow configurations. They are integral solutions of the mass balance equations, including the one representing transfer across the membrane. Salt passage is assumed to be zero but allowance is made for concentration polarisation. The solutions presented obviate the need for approximations based upon a log mean driving force which are only mere approximations when there is transfer of mass from one side of the transfer surface to the other. Secondly a comparison between the estimates of areas using a log-mean approximation and the calculated areas using the analytical solution shows that the former will generate significant errors at high recoveries for the case of counter-current flow. Thirdly the potential recovery is also elucidated for various combinations of salinity, flow rate ratios and flow arrangement.

Keywords: Forward Osmosis; Membrane area; Desalination; effectiveness

Highlights (to be uploaded separately)

Exact solutions for sizing ideal Forward Osmosis membrane systems

Solutions include allowance for concentration polarisation

Limitations on use of log-mean driving force demonstrated for a range of conditions

Large difference in membrane area for counter-current exchangers at high recoveries

Graphical Abstract (to be uploaded separately): modified version of Fig 3

1. Introduction

The principle of forward osmosis (FO) is based on the osmotic pressure difference between the chemical potential of two fluids, separated by a semi-permeable salt rejecting membrane. The major advantage of FO is that it occurs spontaneously without any external pressure, unlike the case of other pressure-driven membrane processes. The *draw stream* is a concentrated saline solution (generally sea water) and the *feed stream* is generally low in salt concentration (wastewater), facilitating the transport of water from the feed side to the draw solution, by virtue of the osmotic pressure gradient. Over the past few decades, FO has attracted significant attention for its application potential in treatment of industrial wastewater and water reuse [1-4], desalinating seawater [5, 6], food processing [7,8] and power generation by converting the osmotic pressure into hydraulic pressure [8-11]. However it is widely recognised that the water flux in an FO process is severely limited by internal concentration polarization (ICP) which is a term for describing the phenomenon by which there is either dilution of the high-osmotic-pressure draw solution or undesirable concentration of the feed solution inside the FO support structure [12-13] and challenges in designing compact modules have been noted [13-14]. In particular strong doubts were expressed as to whether forward osmosis will ever successfully compete with reverse osmosis for desalination of seawater because of inherent mass transfer limitations [13]. From a solid theoretical analysis it was concluded that the future of forward osmosis probably lies with niche applications of very high salinity brines [13]. In such applications the molar concentrations on both sides of the membrane will be high and in terms of the nomenclature introduced later the ratio $\frac{c_{20}}{c_{10}}$ will be modest, say 1.5 to 3.

In principle the solutions on either side of the membrane can be from natural sources, waste streams or high purity solutions provided a high concentration gradient across the membrane in maintained. However as only one side commercially available membranes are skinned the potential for significant fouling is high [15]. Despite this problem and the limitation of ICP, interest in FO has continued up to the present because it is seen to have potential to contribute to low-energy water and waste-water treatment processes either conventionally [16] or as hybrid FO [17]. However three areas of major improvements remain paramount in the research and design of FO applications [18]. They are (i) optimum membrane morphology to minimize internal concentration polarization; (ii) suitable composition of the draw solution [17, 19] and (iii) module design and configuration. The analysis in this paper contributes to

the third area as it will facilitate the technical and economical evaluation of forward osmosis desalination systems.

The design equations and correlations used to model the mass transport of fluid are generally analogous to corresponding heat-transfer situations. The operation of an osmotic mass exchanger is similar to that of a heat exchanger. Here, it is the temperature difference between the hot and the cold fluid that is the driving force for energy transfer, which is analogous to the osmotic pressure difference, in the case of a FO or pressure retarded osmosis (PRO) system. In the case of PRO, the osmotic pressure is harnessed in the form of hydraulic energy to generate power. The key difference with a FO system is that the driving force is the osmotic pressure in the later while it is the hydraulic pressure difference in the case of PRO.

In a recent study by Mazlan et al. [19], the area required for an FO membrane mass exchanger is calculated using the log-mean-osmotic-pressure-difference by making an analogy with the log-mean-temperature-difference (LMTD), which is widely accepted for heat exchangers. They simply assumed that one could replace the ΔT terms with the corresponding $\Delta\Pi$ terms. Hence:

$$\text{Area} \propto \frac{\ln(\Delta\Pi_f/\Delta\Pi_i)}{\Delta\Pi f - \Delta\Pi_i} \qquad (1)$$

where $\Delta\Pi_f$ is the osmotic pressure difference between the feed and the draw stream at the exit, and $\Delta\Pi_i$ is the osmotic pressure difference at the inlet. The fundamental difference between the two systems (heat and mass exchanger) is that, unlike in a heat exchanger, the transported quantity is not conserved longitudinally in the FO system. Thus, the usage of LMTD analogy for the design of mass-exchanger systems is incorrect.

Now for heat exchanger, the effectiveness-number of transfer units (ε-NTU) method is a popular design method that estimates the required surface area for a fixed effectiveness (ε) and operational parameters. The effectiveness (ε) is the ratio of the actual heat transfer to the maximum heat exchange possible. The number of transfer units determines the effective size of the heat exchanger. In the case of PRO, a modified effectiveness-mass-transfer unit (ε-MTU) method has been developed [20], similar to the ε-NTU analysis in a heat exchanger [21]. Recently Wu *et al.* [22] developed a heat-exchanger (e-NTU) model to evaluate the flux in Direct Contact Membrane Distillation. Their model is applicable for both co- and counter-flow configurations at low feed salinity and operates at small computational cost compared to

finite difference methods. Subsequently others have approximated balanced single-stage Membrane Distillation (MD) systems as counter-flow heat exchangers in order to understand the energetic performance of various MD configurations [23]. The present study is a counterpart to these works and is focused on the design of FO systems from the fundamental overall mass balances. The present work also complements the work of the Lienhard group on Reverse Osmosis (RO) [20] and PRO [24] and analytical solutions for sizing ideal Forward Osmosis membrane systems are developed for both co-current and counter-current flow configurations. Our approach avoids some of the approximations used by others when approximating the process design equations of membrane systems to those of classical chemical engineering systems. As part of the project we identified the regimes or operating conditions where the actual estimated area deviates significantly from the log-mean approximation described by Eq. (1). The closed-form analytical solution for both the co-current and counter-current flow configuration relates the dimensionless performance parameters of the exchanger to the effective design size and input stream properties. The discrepancy in the design area using the log-mean approach and the present integral analysis is quantified. The recovery fraction and the effectiveness, defined as the ratio with respect to the maximum possible recovery are also elucidated in this study.

2. Forward osmosis mass exchanger model

The schematic of the membrane-based mass-exchanger system is presented in Fig. 1. The two streams are separated by a semi-permeable membrane. The flow configuration can be either the same direction (co-current, Fig. 1a) or the opposing direction (counter-current, Fig. 1b). Depending on the ratio of the concentration of feed to draw solution, the permeation can be in either direction across the membrane (i.e., feed to the draw side, if draw solution is more concentrated, or vice-versa). In general, the feed solution will have a low osmotic pressure compared with the draw solution, which is typically sea water. The inlet and the outlet stream conditions are given in terms of the solution flow rate, salt concentration and osmotic pressure.

Although the effective driving force in any membrane process is mitigated by concentration polarization and for osmotically driven one ICP is important, our model had as its genesis the aim of taking as thorough an approach to the calculation of membrane area for an ideal FO systems as others [24] did with an ideal PRO and hence show the

inappropriateness of using a LMTD approach as developed elsewhere [19]. Thus initially an assumption was made to neglect concentration polarisation effects. However due to the ICP self-compensation effect discussed in Appendix A an approximate but appropriate allowance can be made for concentration polarisation, which is why we introduce *k* as an overall membrane permeability coefficient rather than use the classic *'A'* parameter to which it is linked but it is not identical to it. With regard to salt passage the analysis in Appendix B shows that its effect upon sizing is very minor. On a strict basis our assumptions can be listed as:

(i) Concentration polarization effects are neglected so the salt concentration at the membrane surface is assumed to be equal to the bulk concentration.

(ii) The membrane is completely salt rejecting in nature, so that pure water flows across the membrane.

(iii) Within the operating salinity range of the FO system, the osmotic pressure is linearly proportional to the salt concentration following van't Hoff's correlation.

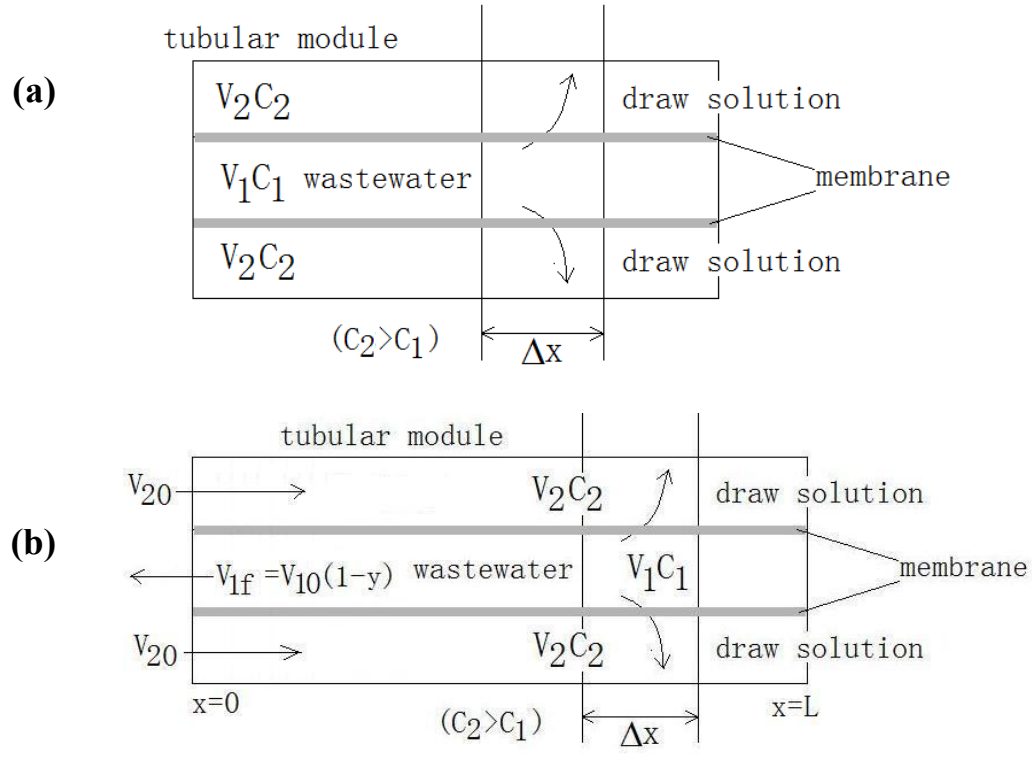

Fig. 1: Schematic showing the system arrangement and process condition, (a) co-current, parallel flow configuration and (b) counter-current, opposing flow configuration. Here 1 represents the feed stream while 2 denote the draw stream. The subscript 0 refers to the inlet

condition and *f* is the outlet stream conditions. The salt concentration and the stream cross-flow rates are represented by *C* and *V*, respectively. The length of the module is *L*.

2.1 Co-current flow configuration

Considering an overall mass balance around the thin tubular section Δx in Fig. 1a, reveals,

$$-\frac{dV_1}{dx} = \frac{dV_2}{dx} = (2\pi r)k[\Pi(c_2) - \Pi(c_1)] \quad (2)$$

where k is the overall membrane permeability coefficient for water and Π is the osmotic pressure of the solution stream. The justification of the use of k and its link to the commonly used 'A' value is given in the Appendix A. Since, for the salt (electrolyte) solution, $\Pi = ic$, where i is the van't Hoff's proportionality constant, Eq. (1) can be simplified as,

$$\frac{dV_2}{dx} = (2\pi r)K(c_2 - c_1) \quad (3)$$

where K is the product of the permeability k and van't Hoff's proportionality constant i. This constant is often written as $\beta R_g T$, as mentioned in Appendix A.

Considering the overall mass balance on the entire FO system, the local concentration c_1 and c_2 in the module is defined as,

$$c_2 = c_{20}\frac{V_{20}}{V_2};\ c_1 = c_{10}\frac{V_{10}}{V_1} \text{ and } V_1 + V_2 = V_{10} + V_{20} \quad (4)$$

where the subscript '0' refers to the inlet condition. Substituting Eq. (4) into Eq. (3) leads to the following differential equation,

$$\frac{dV_2}{dx} = (2\pi r)K\left(\frac{c_{20}V_{20}}{V_2} - \frac{c_{10}V_{10}}{V_{10}+V_{20}-V_2}\right) \quad (5)$$

bounded by the conditions:

$$x = 0;\ V_2 = V_{20} \text{ and for } x = L;\ V_2 = V_{20} + \phi V_{10} \quad (6)$$

where $\phi\ \epsilon\ [0,1)$ corresponds to the amount of recovery. The differential equation (Eq. 5) is integrated with the limits specified in Eq. (6) and is expressed as,

$$\frac{1}{2}\phi^2 V_{10}^2(c_{20}V_{20}+c_{10}V_{10})^2+\phi V_{10}(c_{20}V_{20}^2-c_{10}V_{10}^2)(c_{20}V_{20}+c_{10}V_{10})-$$
$$c_{10}c_{20}V_{10}V_{20}(V_{10}+V_{20})^2\ln\left[1-\phi\left(\frac{c_{20}V_{20}+c_{10}V_{10}}{c_{20}V_{20}-c_{10}V_{20}}\right)\right]=(c_{20}V_{20}+c_{10}V_{10})^3K\xi \qquad (7)$$

where $\xi=(2\pi rL)$ is the membrane area required to obtain a particular recovery ϕ for a given set of stream flow rate, salinity and membrane permeability. It may be noted here that for FO systems using flat sheet membranes, the membrane surface area would be $\xi=WL$ (instead of $2\pi rL$) where W is the width of the membrane surface. Eq. (7) can be categorised into the following cases of interest:

Case 1: when $c_{10}=0$ and $V_{10}=V_{20}$, $\frac{c_{20}}{V_{20}}K\xi=\frac{1}{2}\phi^2+\phi$ (8.1)

Case 2: when $c_{10}=0$ but $V_{10}\neq V_{20}$, $\frac{1}{2}\phi^2\frac{V_{10}}{V_{20}}+\phi=\frac{c_{20}}{V_{10}}K\xi$ (8.2)

Case 3: when $c_{10}\neq 0$ and $V_{10}=V_{20}$,

$$\frac{1}{2}\phi^2(c_{20}+c_{10})^2+\phi(c_{20}^2-c_{10}^2)-4c_{10}c_{20}\ln\left(1-\phi\frac{c_{20}+c_{10}}{c_{20}-c_{10}}\right)=\frac{1}{V_{20}}(c_{10}+c_{20})^3K\xi \qquad (8.3)$$

Case 4: In the asymptotic limit of $V_{20}\gg V_{10}$ and $c_{10}\neq 0$,

$$\phi c_{20}V_{10}(c_{20}+(V_{10}/V_{20})c_{10})-c_{10}c_{20}V_{10}\left(1+2\frac{V_{10}}{V_{20}}\right)\ln\left[1-\phi\left(\frac{c_{20}+(V_{10}/V_{20})c_{10}}{c_{20}-c_{10}}\right)\right]=$$
$$\left[c_{20}+\left(\frac{V_{10}}{V_{20}}\right)c_{10}\right]^3K\xi \qquad (8.4)$$

When using the log-mean osmotic pressure difference approach (Eq. 1), the predicted area required to recover a volume ϕV_{20} is,

$$\xi_{LM}=\frac{1}{k}(\phi V_{20})\frac{\ln(\Delta\Pi_i/\Delta\Pi_f)}{\Delta\Pi_i-\Delta\Pi_f} \qquad (9)$$

which is analogous to the area in a heat exchanger, computed using $\dot{Q}=U\xi\Delta T_{lm}$. The quantities $\Delta\Pi_i$ and $\Delta\Pi_f$, represents osmotic pressure at the inlet and exit stream conditions. Therefore, $\Delta\Pi_i\propto c_{20}$ and $\Delta\Pi_f\propto c_2\propto\frac{1}{1+\phi}c_{20}$ as determined from Eq. (4), we obtain Eq. (10) as,

$$\xi_{LM}=(1+\phi)\ln(1+\phi)\left(\frac{V_{20}}{c_{20}K}\right) \qquad (10)$$

Another simple but less accurate way to calculate the mean difference is the arithmetic mean difference (AMTD) defined as the difference between the average of the inlet and outlet temperature of two streams. In the case of the membrane area based on the arithmetic mean, analogous to the AMTD for heat exchanger, is expressed as,

$$\xi_{AM} = \frac{1}{k}(\phi V_{20})\frac{2}{\Delta\Pi_i + \Delta\Pi_f} = 2\phi\left(\frac{1+\phi}{2+\phi}\right)\left(\frac{V_{20}}{c_{20}K}\right) \quad (11)$$

In the situation corresponding to the simplest case 1 (of zero salinity in the feed), the membrane area required for the 75% recovery $\left(\phi = \frac{3}{4}\right)$ is,

$$\xi = \left(\phi + \frac{1}{2}\phi^2\right)\left(\frac{V_{20}}{c_{20}K}\right) = 1.031\left(\frac{V_{20}}{c_{20}K}\right) \quad (12)$$

whereas, it is equal to $\xi_{LM} = 0.979\left(\frac{V_{20}}{c_{20}K}\right)$ and $\xi_{AM} = 0.954\left(\frac{V_{20}}{c_{20}K}\right)$ using the log-mean osmotic pressure difference and arithmetic mean difference, respectively.

The design area required for a particular extent of recovery for the different methods: log-mean and arithmetic mean difference is illustrated in Fig. 2. The figure clearly shows that the actual area computed from the integral analysis is under represented compared to the other approaches. The deviation is not significant for up to 90% recovery, as it is only 5.5% for the log-mean difference and 7.9% for the arithmetic-mean difference. We note that for the case of arithmetic-mean difference, the deviation in the design area is larger as the magnitude of log-mean difference is smaller than the arithmetic-mean [21]. The arithmetic mean generally gives a satisfactory approximation for the mean osmotic pressure difference when the smallest of the inlet or outlet osmotic pressure differences is more than half the greatest of the inlet or outlet osmotic pressure differences. In the present situation (*case 1*), the difference of the concentration between the feed and draw solution is large $\left(\frac{c_{20}}{c_{10}} \to \infty \text{ or } c_{10} = 0\right)$ which leads to under-representation of the actual design area, unlike the case when $\frac{c_{20}}{c_{10}}$ is finite or $c_{10} \neq 0$, as explained in Fig. 3. Then the actual design area would be more than that calculated using the log-mean approximation, i.e. use of the log-mean approximation would underestimate the area required.

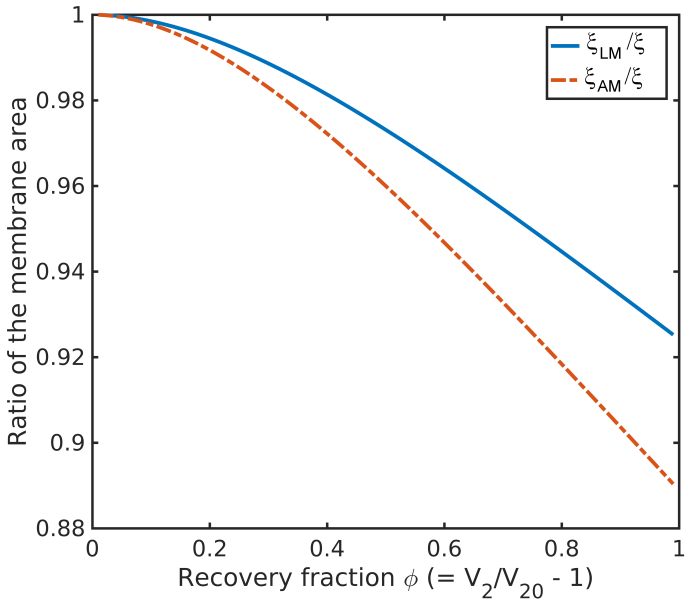

Fig. 2: Area calculated from the log-mean and arithmetic approach is an under-representation compared to that from the present method when $c_{10} = 0$ and $V_{10} = V_{20}$ (case 2).

2.2 Counter-current flow configuration

The overall mass balance on the entire FO system in the counter-current flow situation is expressed as,

$$V_1 + V_{20} = V_{10}(1 - \phi) + V_2 \tag{13}$$

Substituting Eq. (13) into Eq. (3) leads to the following differential equation,

$$\frac{dV_2}{dx} = (2\pi r)K\left[\frac{c_{20}V_{20}}{V_2} - \frac{c_{10}V_{10}}{V_2 - V_{20} - V_{10}(1-\phi)}\right] \tag{14}$$

bounded by the conditions: $x = 0;\ V_2 = V_{20}$ and for $x = L;\ V_2 = V_{20} + yV_{10}$

The solution to Eq. (14) can be represented as,

$$\frac{1}{2}\phi^2 V_{10}^2(c_{20}V_{20} - c_{10}V_{10})^2 + \phi V_{10}(c_{20}V_{20} - c_{10}V_{10})[c_{20}V_{20}^2 - c_{10}V_{10}^2(1-\phi)] + c_{10}c_{20}V_{10}V_{20}[V_{20} - V_{10}(1-\phi)]^2 \ln\left[1 + \frac{\phi(c_{20}V_{20} - c_{10}V_{10})}{c_{20}V_{20}(1-\phi) - c_{10}V_{20}}\right] = (c_{20}V_{20} - c_{10}V_{10})^3 K\xi \tag{15}$$

Similar to the co-current instance, Eq. (15) can be simplified for four different operating conditions as follows,

Case 1: when $c_{10} = 0$ and $V_{10} = V_{20}$, $\frac{1}{2}\phi^2 + \phi = \frac{c_{20}}{V_{20}} K\xi$ (16.1)

Case 2: when $c_{10} = 0$ but $V_{10} \neq V_{20}$, $\frac{1}{2}\phi^2 \frac{V_{10}}{V_{20}} + \phi = \frac{c_{20}}{V_{10}} K\xi$ (16.2)

Note that these two cases are the same as for the co-current flow configuration. This suggests when the salt concentration (or the osmotic pressure) in the feed stream is zero, the extent of recovery is same for co- and counter-current flow arrangements, with the same membrane area.

Case 3: when $c_{10} \neq 0$ and $V_{10} = V_{20}$,

$$\frac{1}{2}y^2(c_{20} - c_{10})^2 + \phi(c_{20} - c_{10})[c_{20} - c_{10}(1 - \phi)] + c_{10}c_{20}y^2 ln\left[1 + y\frac{c_{20} - c_{10}}{c_{20}(1-\phi) - c_{10}}\right] = \frac{1}{V_{20}}(c_{20} - c_{10})^3 K\xi \quad (16.3)$$

Case 4: when $c_{10} \neq 0$ and $V_{20} \gg V_{10}$,

$$\phi c_{20}V_{10}[c_{20} - (V_{10}/V_{20})c_{10}] + c_{10}c_{20}V_{10}\left[1 + 2(1 - \phi)\frac{V_{10}}{V_{20}}\right]^2 ln\left[1 + \phi\left(\frac{c_{20} - (V_{10}/V_{20})c_{10}}{c_{20}(1-\phi) - c_{10}}\right)\right] = \left[c_{20} - \left(\frac{V_{10}}{V_{20}}\right)c_{10}\right]^3 K\xi \quad (16.4)$$

2.3 Generalised condition

In order to generalize the design equations for the co- and counter-current flow configurations, the variables corresponding to concentration and flow rates are scaled as: $c_{20} = mc_{10}$, where $m \epsilon (1, +\infty)$ and $V_{20} = sV_{10}$, where $s \epsilon (0, +\infty)$. Eq. (7) for the case of co-current flow is then transformed as,

$$\frac{1}{2}\phi^2(sm + 1)^2 + \phi(sm + 1)(s^2m - 1) - sm(1 + s)^2 \ln\left[1 + \phi\frac{sm+1}{s(m-1)}\right] = (sm + 1)^3 \frac{c_{10}}{V_{10}} K\xi \quad (17)$$

Similarly, for a counter-current configuration, Eq. (15) is simplified as,

$$\frac{1}{2}\phi^2(sm - 1)^2 + \phi(sm - 1)(s^2m + \phi - 1) + sm[s - (1 - \phi)]^2 \ln\left[1 + \phi\frac{sm-1}{sm(1-\phi) - s}\right] = (sm - 1)^3 \frac{c_{10}}{V_{10}} K\xi \quad (18)$$

For the case when $c_{10} \neq 0$ but $V_{10} = V_{20}$ (s = 1) for both co- and counter-current configurations, Eqs. (17) and (18) are reduced to

$$\frac{1}{2}\phi^2(m+1)^2 + \phi(m^2-1) - 4m\ln\left[1+\phi\frac{m-1}{m-1}\right] = (m+1)^3\frac{c_{10}}{V_{20}}K\xi \qquad (19)$$

$$\frac{1}{2}\phi^2(m-1)^2 + \phi(m-1)(m+\phi-1) + my^2\ln\left[1+\frac{(m-1)\phi}{m(1-\phi)-1}\right] = (m-1)^3\frac{c_{10}}{V_{20}}K\xi \qquad (20)$$

respectively. In the case of log-mean osmotic pressure difference (for $V_{10} = V_{20}$), the membrane area can be represented by Eqs. (21, 22) for the co-current and counter-current case, respectively,

$$\frac{c_{10}}{V_{20}}K\xi_{LM} = y(1-\phi^2)\frac{\ln[(m-1)(1-\phi^2)/(m(1-\phi)-\phi-1)]}{[m(1+\phi)-\phi^2(m-1)]} \qquad (21)$$

$$\frac{c_{10}}{V_{20}}K\xi_{LM} = y(1-\phi^2)\frac{\ln[(m-1-\phi)(1-\phi)/(m(1-\phi)-1)(1+\phi)]}{[(m-\phi-1)(1-\phi)-(m(1-\phi)-1)(1+\phi)]} \qquad (22)$$

3. Results and Discussion

Firstly we note that whilst we were principally concerned with the ideal case – see our assumptions at the beginning of section 2 – a check was made to ascertain whether salt passage would impact significantly upon the analysis. It was established (see the Appendix B for details) that the effect would be a second order one.

In mass as well as energy exchange, counter-current flow is often superior to a co-current configuration [21]. In a counter-current mechanism, a gradual spatial gradient of the osmotic pressure is maintained through the unit. In the co-current arrangement, the initial gradient is higher but falls off drastically, and is responsible for the wasted average potential. A typical example is the case of a bubble distillation column, the vapours of the volatile component bubbles through the downward liquid resulting in maximum mass exchange. For the given membrane area, a higher recovery is obtained in case of a counter-current flow arrangement [21], as evident from Fig. 3. This figure clearly delineates the discrepancy between the log-mean with the present approaches. The deviation increases with the extent of recovery as can be inferred from the figure. The degree of maximum possible recovery can be augmented with the concentration of the draw solution, leading to high deviation between the two

calculated areas. However, for a fixed recovery fraction, the difference between the two areas is magnified in the case of co-current flow configuration. Note that we can identify the curve corresponding to $c_{20}/c_{10} = \infty$, as zero feed salinity (zero feed osmotic pressure), which corresponds to case 2, $c_{10} = 0$, and the co- and counter-current flow configuration have identical result as expected. For up to 60% of the maximum possible recovery fraction, the log-mean calculation fares well with the integral analysis (within 5% deviation). For example, corresponding to $c_{20}/c_{10} = 5$, the maximum recovery is 0.8 for counter-current flow configuration, the ratio $\xi_{LM}/\xi \in (0.95, 1.05)\ \forall\ \phi < 0.48$. In most practical applications, the ratio of c_{20}/c_{10} generally varies from 2 to 10.

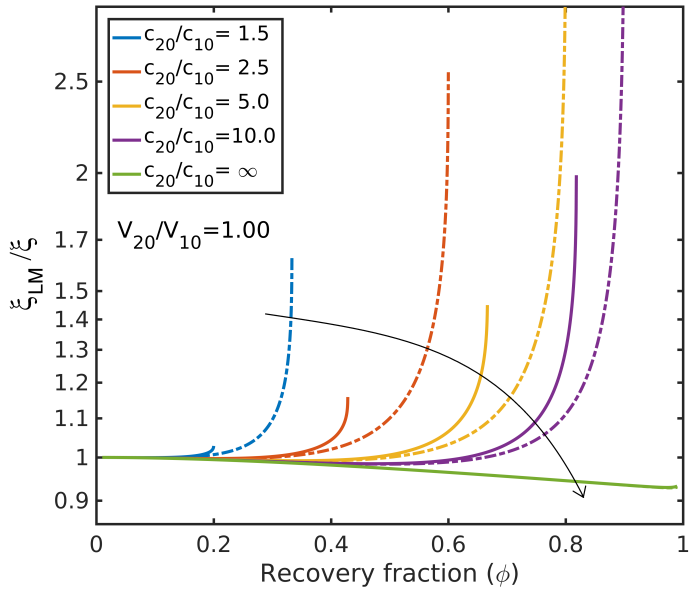

Fig. 3: Ratio of the area calculated from the log-mean approach and the present analysis using Eqs. (19-22). Dashed lined for counter-current flow while solid lines for co-current flow. The arrow represent the increasing c_{20}/c_{10} ratio in the order of 1.5, 2.5, 5, 10 and ∞.

In Fig. 4 the membrane design area, scaled as $\xi_0 = \frac{c_{10}}{V_{20}} K\xi$, is represented as a function of the ratio of the draw to feed salinity with the ratio of the volumetric flow rates as a parameter. Input was calculated from the design equation represented in Eq. (17) and Eq. (18) for the parallel and counter-current flow arrangement. As expected the membrane area required to attain a desired recovery increases as the concentration difference between the feed and draw stream diminishes or with increasing feed flow rate compared to the flow rate of the draw solution. The membrane area required is comparatively less for the case of counter-current flow compared to that for the parallel flow arrangement.

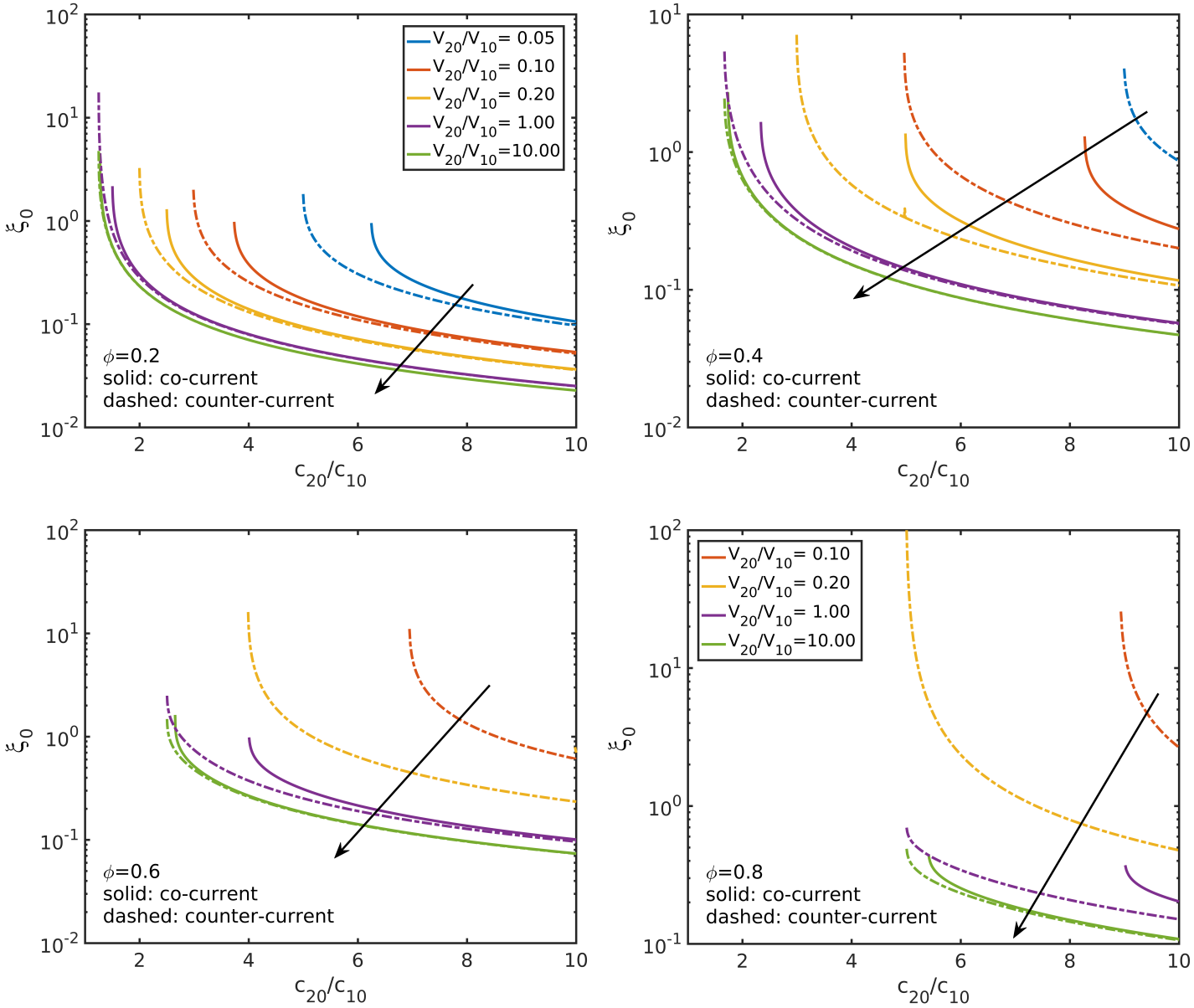

Fig. 4: Membrane area as a function of the relative feed concentration calculated from the present integral analysis with variation of the relative cross-flow rates and fractional recovery. The direction of the arrow represents increasing ratio of V_{20}/V_{10} as 0.05, 0.1, 0.2, 1 and 10. For the figures corresponding to ϕ = 0.6 and ϕ = 0.8, the arrows represent the increasing ratio of V_{20}/V_{10} as 0.1, 0.2, 1 and 10.

The performance of the FO system can be quantified in terms of the recovery fraction obtained for a specific set of operating conditions (Figure 5). In the case of the counter-current exchange, higher water recovery is obtained as expected. Interestingly, the difference in the recovery between co and counter-current flow arrangement is greater for equal stream flow rates (V_{20}/V_{10} = 1) when the salinity ratio of the two streams is smaller. As the salinity of the draw solution is increased, the difference of the recovery fraction between the two flow

arrangements enhances with the flow rate of the feed solution. This is because, in a counter-current mass exchanger, the mean difference between the inlet and outlet concentration is a minimum for equivalent mass flow rates of the two streams and smaller differences in the salinity levels. The counter-current flow arrangement is distinctively advantageous under two circumstances. Firstly when the flow rates of the two streams are equal (and the salinity ratio is less than 2.5) it is particularly advantageous; see Figure 5 for $c_{20}/c_{10} = 1.5$ and $c_{20}/c_{10} = 2.5$. (The lines are in purple.) Secondly for the combination of c_{20}/c_{10} being large and $V_{20}/V_{10} < 1$ (i.e. the salinity of the draw solution is relatively high with respect to the that of the feed and the feed flow rate is higher than that of the draw) the counter-current flow arrangement gives particularly higher recoveries for ξ_0 values of over 0.5 - ξ_0 is the scaled membrane design area as defined above.

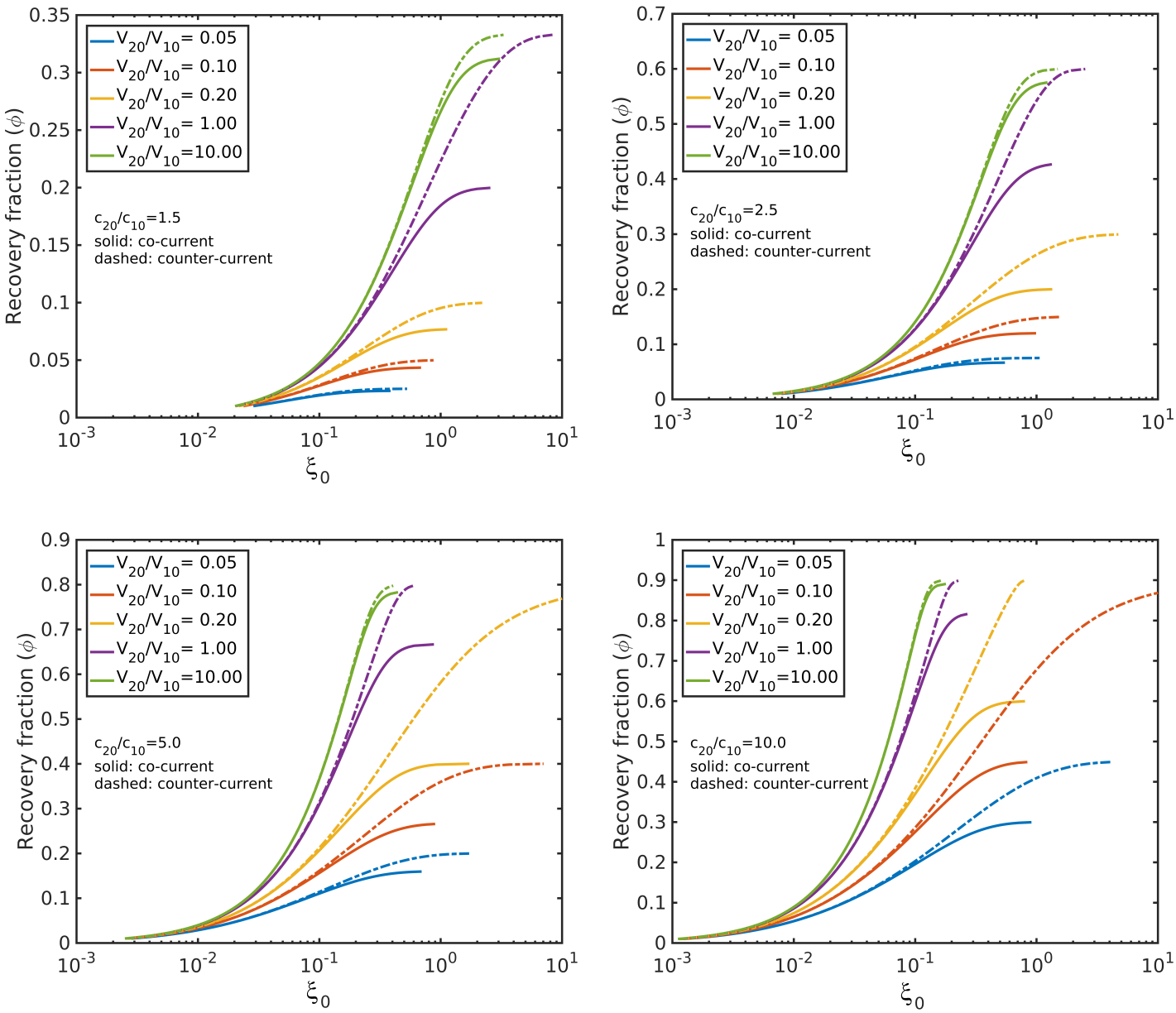

Fig. 5: Recovery fraction as a function of the membrane area calculated from the integral analysis with variation of the relative feed concentration with relative cross-flow rates as the parameter.

The effectiveness of the membrane mass exchanger can be defined as the $\varepsilon = \frac{\phi}{\phi_{max}}$ [24]. However, the efficiency of the process determined from the effectiveness parameter, ε can be misleading in comparing co-current and counter-current flow arrangements. Noting from Figure 6, the counter-current exchanger resembles low ε compared to the co-current flow. This is primarily because as the maximum absolute recovery higher in the case of

counter-current flow, as illustrated in Figure 5. Figure 6 also establishes the fact that for small difference between the salinities of the two streams, maximum change in the performance efficiency of co- and counter-current exchanger is observed when the cross-flow rates of the streams are equal. On the contrary, for high salinity draw solution, the maximum change in the performance between the flow configurations is visible for relatively higher feed flow rates but for V_{20}/V_{10}= 10 and c_{20}/c_{10}=10 the lines for counter-current and co-current flow are imposed upon one another; see right-hand pane in Figure 6.

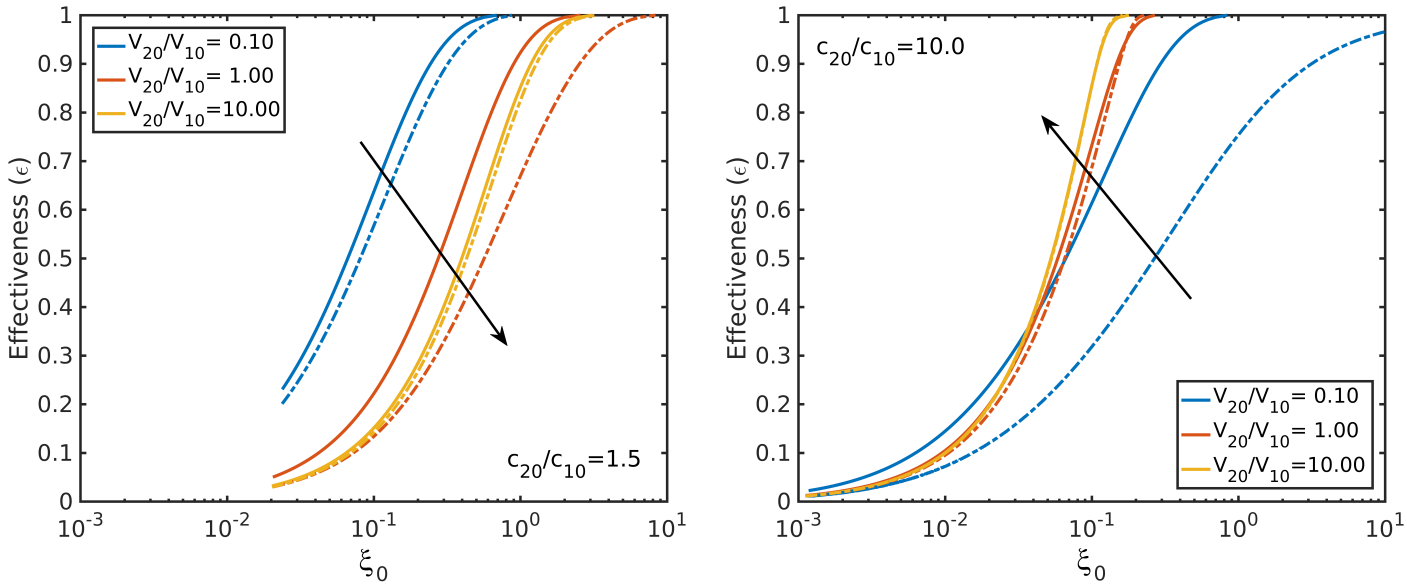

Fig. 6: Effectiveness of the separation process for different cross-flow rates and concentration ratios. Dashed lines for the counter-current flow arrangement; solid lines for the co-current flow. The arrow represents the increasing ratio of the V_{20}/V_{10} as 0.1, 1 and 10. However, it may be noted that in the left figure (c_{20}/c_{10} = 1.5), the effectiveness of the co- and counter-current process for V_{20}/V_{10} = 10 is more than the counter-current case for V_{20}/V_{10} = 1.

Concluding Remarks

Unlike some recent publications [25, 26] comparing the energy consumption of FO–RO hybrid processes with a standalone RO process from a thermodynamic perspective, assuming idealized conditions, Mazlan et al [19] did include process details such as pressure drop and pretreatment in their detailed analysis. However, as mentioned above, they calculated specific membrane area requirements using equation (1). The present analysis has shown that this approximation is unnecessary. Additionally the conditions under which the discrepancy from

using the log-mean approach is significant compared to the detailed integral analysis developed above have been identified. Ultra large scale projects such as those outlined in [17], the Mega-ton Water System [25] and Seawater High Efficiency Reverse Osmosis O&M Research, i.e. SeaHERO2 [26] need accurate methods for estimating the membrane area requirements, including that of FO modules as these might be part of the overall plant.

The log-mean approximation deviates away from the actual estimates significantly for the case of counter-current flow arrangement and at high recoveries. Interestingly, the actual design area is under represented by the log-mean approximation when the ratio of the feed salinity to the draw solution is more than 1 and appreciable differences are observed for values of the ratio more than 2.

This work (as with similar work on RO and PRO [20, 24]) is limited an idealization with regard to concentration polarization. However unlike those papers the assumption that concentration polarisation is absent has not been made but there is a restriction; the allowance made is to assume that its influence is uniform throughout a module. As the modules are assumed to have an ALFS orientation the ICP self-compensation effect will be manifest and so the assumption of an invariant overall permeability coefficient k is reasonable, which permits due allowance for concentration polarisation.

The present study has elucidated the potential recovery for various combinations of salinity, flow rate ratios and flow arrangement and highlighted the conditions under which counter current flow are particularly advantageous. These include process designs in which the inlet flowrates of feed and draw are equal. Overall not only have we clearly highlight the key mathematical inconsistency arising from the employment of the LMTD analogy in the design of FO processes but have provided a practical alternative.

Acknowledgements

We are thankful to Dr Ian Griffiths (Mathematical Institute, University of Oxford, UK) for the helpful discussions during the course of the work. Sourav Mondal is thankful to the Royal Society for funding the position at University of Oxford. We are grateful to the reviewer whose useful suggestion prompted the production of the Appendices.

References

[1] T.Y. Cath, A.E. Childress, M. Elimelech, Forward osmosis: Principles, applications, and recent developments, J. Membr. Sci. 281 (2006) 70-87.

[2] K.L. Hickenbottom, N.T. Hancock, N.R. Hutchings, E.W. Appleton, E.G. Beaudry, P. Xu, T.Y. Cath, Forward osmosis treatment of drilling mud and fracturing wastewater from oil and gas operations, Desalination 312 (2013) 60-66.

[3] B.D. Coday, P. Xu, E.G. Beaudry, J. Herron, K. Lampi, N.T. Hancock, T.Y. Cath, The sweet spot of forward osmosis: treatment of produced water, drilling wastewater, and other complex and difficult liquid streams, Desalination 333 (2014) 23-35.

[4] K. Lutchmiah, A.R.D. Verliefde, K. Roest, L.C. Rietveld, E.R. Cornelissen, Forward osmosis for application in wastewater treatment: a review, Wat. Res. 58 (2014) 179-197.

[5] R.V. Linares, Z. Li, S. Sarp, S.S. Bucs, A. Amy, J.S. Vrouwenvelder, Forward osmosis niches in seawater desalination and wastewater reuse, Wat. Res. 66 (2014) 122-139.

[6] C. Boo, M. Elimelech, S. Hong, Fouling control in a forward osmosis process integrating seawater desalination and wastewater reclamation, J. Membr. Sci. 444 (2013) 148-156.

[7] V. Sant'Anna, L.D.F. Marczak, I.C. Tessaro, Membrane concentration of liquid foods by forward osmosis: Process and quality view, J. Food Eng. 111 (2012) 483-489.

[8] S. Zhao, L. Zou, C.Y. Tang, D. Mulcahy, Recent developments in forward osmosis: opportunities and challenges, J. Membr. Sci. 396 (2012) 1-21.

[9] B.E. Logan, M. Elimelech, Membrane-based processes for sustainable power generation using water, Nature 488 (2012) 313-319.

[10] T.S. Chung, X. Li, R.C. Ong, Q. Ge, H. Wang, G. Han, Emerging forward osmosis (FO) technologies and challenges ahead for clean water and clean energy applications, Curr. Opn. Chem. Eng. 1 (2012) 246-257.

[11] T.S. Chung, S. Zhang, K.Y. Wang, J. Su, M.M. Ling, Forward osmosis processes: yesterday, today and tomorrow, Desalination 287 (2012) 78-81.

[12] C.Y. Tang, Q. She, W.C.L. Lay, R. Wang, R. Field, A.G. Fane, Modeling double-skinned FO membranes, Desalination 283 (2011) 178–186.

[13] R.W. Field, J.J. Wu, Mass transfer limitations in forward osmosis: Are some potential applications overhyped?, Desalination 318 (2013) 118–124.

[14] B. Van der Bruggen, P. Luis, Forward osmosis: understanding the hype, Rev. Chem. Eng. 31 (2014) 11-20. DOI 10.1515/revce-2014-0033.

[15] Q. She, R. Wang, A.G. Fane, C.Y. Tang, Membrane fouling in osmotically driven membrane processes: A review, J. Membr. Sci. 499 (2016) 201–233.

[16] Y. Kim, J.H. Lee, Y.C. Kim, K.H. Lee, I.S. Park, S.-J. Park, Operation and simulation of pilot-scale forward osmosis desalination with ammonium bicarbonate, Chem. Eng. Res. Design 94 (2015) 390–395.

[17] L. Chekli, S. Phuntsho, J.E. Kim, J. Kim, J.Y. Choi, J.-S. Choi, S. Kim, J.H. Kim, S. Hong, J. Sohn, H.K. Shon, A comprehensive review of hybrid forward osmosis systems: Performance, applications and future prospects, J. Membr. Sci. 497 (2016) 430–449.

[18] Q. Ge, M. Ling, T.-S. Chung, Draw solutions for forward osmosis processes: Developments, challenges, and prospects for the future, J. Membr. Sci. 442 (2013) 225-237.

[19] N.M. Mazlan, D. Peshev, A.G. Livingston, Energy consumption for desalination—A comparison of forward osmosis with reverse osmosis, and the potential for perfect membranes, Desalination 377 (2016) 138-151.

[20] L.D. Banchik, M.H. Sharqawy, J.H. Lienhard V, Effectiveness–mass transfer units (ε–MTU) model of a reverse osmosis membrane mass exchanger, J. Membr. Sci. 458 (2014) 189-198.

[21] F.P. Incropera, D.P. DeWitt, Introduction to heat transfer, 4th ed., 2002, John Wiley and Sons: New York.

[22] H.Y. Wu, M. Tay, R.W. Field, Novel method for the design and assessment of direct contact membrane distillation modules, J. Membr. Sci. 513 (2016) 260-269.

[23] J. Swaminathan, H.W. Chung, D.M. Warsinger, J.H. Lienhard V, Membrane distillation model based on heat exchanger theory and configuration comparison, Appl. Energy 184 (2016) 491–505.

[24] M.H. Sharqawy, L.D. Banchik, J.H. Lienhard V, Effectiveness–mass transfer units (ε–MTU) model of an ideal pressure retarded osmosis membrane mass exchanger, J. Membr. Sci. 445 (2013) 211-219.

[25] http://www.desaltech2015.com/assets/presenters/Kurihara_Masaru.pdf accessed Nov 19th 2016.

[26] S. Kim, B.S. Oh, M.H. Hwang, S. Hong, J.H. Kim, S. Lee, I.S. Kim, An ambitious step to the future desalination technology: SEAHERO R&D program (2007–2012), Appl. Water Sci. 1 (2011) 11-17. doi:10.1007/s13201-011-0003-4

Appendix A – Justification of equation (2) and allowance for concentration polarisation

The relationship between the proportionality constant k in equation (2) and the commonly used 'A' parameter is given below. It will be recalled that consideration of an overall mass balance around the thin tubular section Δx in Fig. 1a, yielded

$$-\frac{dV_1}{dx} = \frac{dV_2}{dx} = (2\pi r)k[\Pi(c_2) - \Pi(c_1)] \qquad (2)$$

where k is the membrane permeability coefficient for water and the two osmotic pressure terms are the bulk values for the two streams. Now for FO membranes with the active layer facing the feed (ALFS) the flux equation, in the absence of fouling, can be written as [15]:

$$J_w = A\left[\left(\pi_{ds} - \pi_{fs}\right) - F_{dcp}\left(\pi_{ds} + \frac{J_s}{J_w}\pi R_g T\right) - F_{fcp}\left(\pi_{fs} + \frac{J_s}{J_w}\pi R_g T\right)\right] \qquad (A1)$$

where π_{ds} and π_{fs} are the osmotic pressure of the draw and feed solutions respectively; J_w and J_s are respectively the volumetric flux of the water and the mass flux of the salt. The term $\pi R_g T$ is the pressure per unit concentration with π being the ratio of the actual concentration of particles produced when the solute is dissolved to the concentration of the particles based upon the actual mass and the molar mass of the solute. For NaCl the factor is 2 whereas for non-electrolytes dissolved in water it would be essentially one.

The terms F_{fcp} and F_{dcp} are factors that approach zero as flux approaches zero. The former is for the feed side where there is concentrative concentration polarisation (i.e. the concentration at the surface of the membrane is higher than in the bulk feed) and the latter is for the draw side where there is dilutive so called "concentration polarisation" (i.e. the concentration at the membrane/support layer interface is lower than in the bulk on the draw side). Mathematically the terms are given by equations (A2) and (A3) are for ALFS orientation.

ALFS orientation $$F_{fcp} = \exp\left(\frac{J_w}{k_f}\right) - 1 \qquad (A2)$$

ALFS orientation: $F_{dcp} = 1 - \exp\left(-\frac{J_w}{K_d}\right)$ (A3)

The mass transfer coefficient in (A2) is that for the channel on the feed side and this can be relatively high but the term K_d in (A3) is adversely influenced by the internal concentration polarisation in the support layer which makes this term small and the correction given by F_{dcp} is always very significant.

It follows from the above equations that

$$k = A\left[1 - F_{dcp}\frac{\left(\square_{ds} + \frac{J_s}{J_w}\square R_g T\right)}{\left(\square_{ds} - \square_{fs}\right)} - F_{fcp}\frac{\left(\square_{fs} + \frac{J_s}{J_w}\square R_g T\right)}{\left(\square_{ds} - \square_{fs}\right)}\right] \quad \text{(A4)}$$

The term $\frac{J_s}{J_w}\square R_g T$ can be approximated to B/A where A and B are the standard parameters for water and salt permeabilities. Now with estimates of the mass transfer coefficients and knowledge of A and B one can for given values of $\square_{ds}$ and $\square_{fs}$ estimate the flux J_w using equation (A1). The terms F_{dcp} and F_{fcp} can then be calculated using equations (A2) and (A3) and hence k can then be obtained from (A4).

Although the term K_d reduces the actual driving force across the active layer significantly below the apparent driving force given by $\square_{ds} - \square_{fs}$, equation (A3) is important in another way; the correction factor brings flux stability. This stability has been labelled as the ICP-self compensation effect. A decrease in $\square_{ds}$ will reduce the flux but this also lead to a smaller values of F_{dcp} and F_{fcp} and so the proportionate reduction in flux will be less than the proportionate reduction in overall driving force. This is particularly true for the ALDS orientation which generates relatively large values of $F_{dcp.}$ The relevance to our establishment of the relationship between the overall proportionality constant k in equation (2) and the commonly used 'A' parameter is that as the recovery increases and the concentrations c_1 and c_2 change (see section 2) the estimated value of k will change but change modestly. We recommend that k be estimated for both ends of a module and an average value used.

Appendix B – The effect of salt leakage

Considering a mass balance for the salt species, accounting for the salt leakage, we can say

$$\bar{V}_1 \frac{dc_1}{dx} = 2\pi r B(c_2 - c_1) \quad \text{(A5)}$$

where $\bar{V}_1$ is the average volume flow rate of the feed solution, and considering that the osmotic pressure follows a linear relationship for low molecular weight solutes (as is the case here), $\Pi = ic$ (i being the van't Hoff's factor). It may be pointed out here that Eq. (3) in the main text is valid when B = 0, no salt leakage as mentioned in the list of assumptions (beginning of section 2). However in this Appendix the differences in the $c_{1L}(c_1, x = L)$ when $B = 0$ (already reported in the original manuscript) and c_{1L} when $B \neq 0$ are investigated for one of the standard cases.

Now let us evaluate c_{1L}/c_{2L} when $B \neq 0$, but $c_{10} \sim 0$ (for simplicity in the demonstration analysis). From the previous analysis we can find

$$\bar{V}_2 = \frac{1}{L}\int_0^L V_2 dx = \frac{1}{3K\xi c_{20} V_{20}}\{\phi^3 V_{10}^3 + 3\phi V_{20} V_{10}(V_{20} + \phi V_{10})\} \quad \text{(A6)}$$

$$\bar{V}_1 = V_{20} + V_{10} - \bar{V}_2 \quad \text{(A7)}$$

where ξ is the membrane area. Now, integrating Eq. (A5) using $c_2 = c_{2L}$, we obtain

$$\frac{c_{1L}}{c_{2L}} = 1 - exp\left(-\frac{\xi B}{V_{10} + V_{20} - \bar{V}_2}\right) \quad \text{(A8)}$$

In the case of $V_{10} = V_{20}$, Eq. (A8) reduces to

$$\frac{c_{1L}}{c_{2L}} = 1 - exp\left[-\frac{3}{2}\frac{\xi B}{V_{20}}\left(\frac{2+\phi}{3-\phi^2}\right)\right] \quad \text{(A9)}$$

It can be immediately inferred that when $B \sim 0$, we recover the situation with no salt leakage ($c_{1L} \sim c_{10} \sim 0$). Interestingly the quantity $\xi B/V_{20}$determines the amount of the salt leakage. In practical cases, with large flow rates and for small B, $\xi B/V_{20} \to 0$, implying the insignificance of salt leakage. For other V_{20}/V_{10} ratios of interest the same conclusion is reached.